water

MDPI

Article

Disintegration Characteristics of Highly Weathered Granite under the Influence of Scouring

Xiyang He [1], Chengyu Liu [1,2,*], Xiangxiang Zhang [1,2,*], Changyu Wu [3] and Zhiyu Weng [4]

[1] College of Zijin Geology and Mining, Fuzhou University, Fuzhou 350116, China; fjzzhexy@163.com
[2] Research Center of Geological Engineering, Fuzhou University, Fuzhou 350116, China
[3] College of Civil Engineering, Fuzhou University, Fuzhou 350116, China; 18940031541@163.com
[4] Fujian Research Center for Tunneling and Urban Underground Space Engineering, Huaqiao University, Xiamen 361021, China; wyswzy8108@163.com
* Correspondence: liuchengyuphd@163.com (C.L.); xxzhang@fzu.edu.cn (X.Z.)

Abstract: In South China, due to climatic factors, highly weathered granite is distributed across a large area and easily disintegrates after encountering water, causing many geological disasters and other problems. To determine the disintegration mechanism of highly weathered granite in South China, disintegration tests were carried out on highly weathered granite in the Fuzhou area under different immersion durations, cycle times, and flow rates, with the help of a self-designed disintegration test device. Moreover, the disintegration mechanism of the highly weathered granite was revealed using nuclear magnetic resonance (NMR) technology. The results demonstrated an increase in the cumulative relative disintegration with prolonged immersion time and the number of dry-wet cycles. Beyond a certain flow rate, the cumulative relative disintegration amount stabilized. There was a strong correlation between the steady disintegration rate and immersion time (or dry-wet cycles). The disintegration process of the highly weathered granite was divided into three stages: rapid, moderate, and stable disintegration. Notably, disintegration primarily occurred around the large pores. This study revealed that the variation in the immersion time (or wet-dry-scouring cycles) was fundamentally linked to changes in the relative volume of the large pores in the rock samples. These findings provide valuable insights for predicting and mitigating surface disasters on highly weathered granite slopes.

Keywords: highly weathered granite; disintegration; disintegration steady flow rate; dry-wet cycles; immersion time

Citation: He, X.; Liu, C.; Zhang, X.; Wu, C.; Weng, Z. Disintegration Characteristics of Highly Weathered Granite under the Influence of Scouring. *Water* **2024**, *16*, 496. https://doi.org/10.3390/w16030496

Academic Editors: Yu Huang and Achim A. Beylich

Received: 22 November 2023
Revised: 16 January 2024
Accepted: 24 January 2024
Published: 3 February 2024

1. Introduction

In southern China, there is a large area and depth of thick and highly weathered granite slopes with a thickness distribution of 20 to 60 m [1,2]. Highly weathered granite is a soft rock mass mixed with soil and rock, and its engineering properties are very complicated. Under the action of rainfall, with increasing rainfall duration, the immersion time of highly weathered granite in water increases, water-rock interactions intensify, and the loss of granular cement breaks down [1,2]. Moreover, when the rainfall intensity is high, slope runoff with different flow rates occurs on different parts of the slope surface, particles that have not yet disintegrated but have poor cementation are constantly stripped from the parent body, and disintegration further intensifies, resulting in the formation of different degrees of slope damage [3], as shown in Figure 1. Therefore, the disintegration of highly weathered granite under the action of rainfall is the result of the combined action of water-rock interactions and water erosion. To further study the failure law and mechanism of highly weathered granite under the action of rainfall, it is necessary to study the disintegration law under different flow rates.

Figure 1. Erosion failure of heavily weathered granite slope.

Domestic and international scholars have conducted numerous studies on the disintegration characteristics of soft rocks. It is widely accepted that the disintegration of soft rocks arises from a combination of intrinsic factors [4], such as the structural composition of soft rocks, the type of cement, and the content of clay minerals, along with various complex external factors [5–8], such as rainfall, temperature [8–12], and external stress states. To investigate the disintegration mechanism of soft rocks subjected to dry and wet cycling, researchers such as Wu et al. [9], Dhakal et al. [10], and Chai et al. [11], among others, have conducted indoor experiments. Their findings have revealed a close correlation between the variability of mudrock disintegration and the clay mineral content and the fracture structure within the rock samples. Moreover, Erguler et al. [12] argued that a sole focus on variations in mineral constituents and their contents has limitations in understanding the disintegration law of rocks. Zhang et al. [7] carried out a series of indoor tests to examine the relative contributions of different climatic processes to rock disintegration properties. Disintegration under dry-wet cycles [13,14], freeze-thaw cycles [8], and various hydrothermal conditions [15–17] has been explored, and the influence patterns of humidity, temperature, and other factors on rock disintegration properties have been studied. In addition, Zhang et al. [18,19] also summarized the prevailing test methods for rock disintegration, including immersion disintegration tests, dynamic disintegration tests in disintegration-resistant apparatuses, and in situ disintegration tests. The disintegration tests were conducted by employing different test devices, rock sample sizes, and varying drying temperatures to explore the impact of test methodologies on rock disintegration. However, it is worth noting that in the aforementioned studies, the scholars primarily concentrated on rock disintegration caused by water-rock interactions and did not consider the influence of water scouring. This omission prevented the comprehensive simulation and understanding of how rainfall affects the degradation of the top layer of rock and soil on slopes.

Many scholars have devoted their attention to studying the damage patterns of geotechnical bodies on slopes subjected to water scouring. Zhao et al. [20] demonstrated that geotechnical particles undergoing water scouring are primarily influenced by the water uplift force, water drag force, underwater gravitational force of particles, and interparticle bonding force. They derived the formula for the critical flow rate at which geotechnical particles commence moving within a water flow, predicated on the principles of mechanical equilibrium. Wang et al. [21] devised a scour initiation test device to experimentally investigate the initiation phenomenon of geotechnical particles on slopes exposed to water flow conditions. Their findings indicated that the initiation flow rate of geotechnical particles is predominantly affected by the dry density, clay particle content, and slope gradient. Wu et al. [22] scrutinized the scour damage process of slopes under various rainfall intensities via indoor slope scour tests. Notably, these investigations on the scour damage of geotechnical bodies failed to account for the effects of prior saturation due to varying durations of rainfall and the attenuation of geotechnical particle cementation resulting from differing frequencies of rainfall (multiple wet and dry cycles) before scouring onset. Consequently,

they inadequately simulate and reflect the impact of rainfall on the damage incurred by the surface layer of geotechnical bodies on slopes.

Highly weathered granite is widely distributed along the southeast coast of China, including Hong Kong [1]. These regions experience high temperatures and frequent rainfall, resulting in a humid climate. The highly weathered granite in these areas contains a high internal clay mineral content, increasing susceptibility to softening upon contact with water [4–7]. This vulnerability leads to frequent erosion, mudslides, landslides, and other geological hazards on slopes composed of highly weathered granite [23,24]. Therefore, conducting a comprehensive study on the disintegration characteristics of highly weathered granite under the influence of scouring is of the utmost importance for predicting and preventing geological hazards along the southeastern coast of China and Hong Kong.

This paper introduces a set of disintegration testing equipment capable of maintaining stable and controllable flow rates to address this need. This equipment is designed to conduct disintegration tests on highly weathered granite under varying flow rates, immersion durations, and cycles. By doing so, we aim to establish the relationship between the stable flow rate of disintegration in highly weathered granite, the immersion duration, and the number of cycles. Additionally, we employ nuclear magnetic resonance (NMR) technology to investigate changes in the rock sample pores following scouring and disintegration. This approach allows us to determine the disintegration patterns of highly weathered granite and the underlying mechanisms involved when subjected to scouring effects.

2. Experimental Equipment and Test Method

2.1. Experimental Equipment

A slake durability apparatus is generally used for testing the disintegration of rocks. However, in this study, the fixed speed of the screen drum did not reveal the impact of varying scouring flow rates on rock disintegration. Furthermore, the continuous collisions between the rock samples and the screen drum during rotation lead to rock sample damage, flaking, and deviation in the test results.

To address these limitations and elucidate the disintegration behavior of weathered rock bodies under varying scouring flow rates, this paper presents the design of a scouring disintegration test device with controllable flow rates, as depicted in Figure 2. The test setup comprises a water storage tank, a flow rate adjustment tank, a disintegration tank, and a disintegration particle collection box.

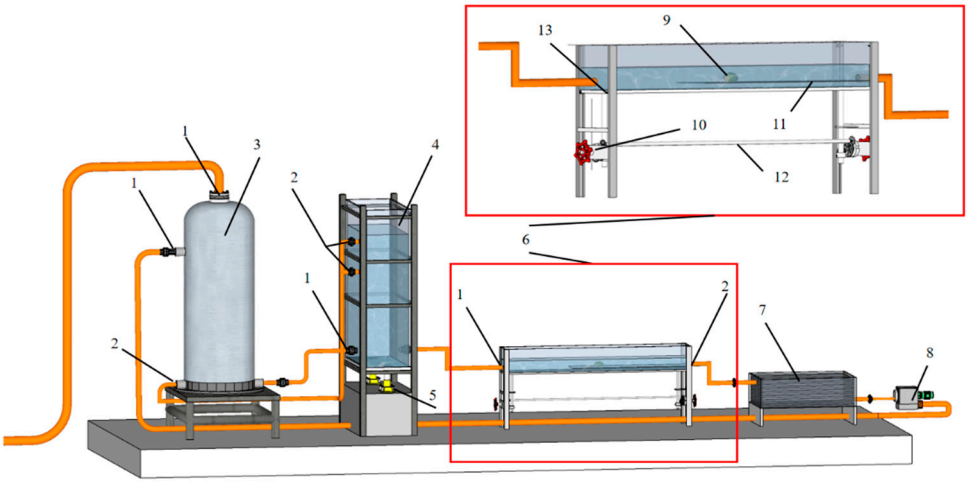

Figure 2. Flow-rate-controlled scouring and disintegration test device.

To simulate the disintegration phenomenon of rock and soil masses on slope surfaces accurately, a disintegration test tank (Figure 2) was designed. The test tank is an open-top glass tank constructed from tempered glass and measures 1920 mm in length, 240 mm in width, and 240 mm in height. The rock sample was positioned at the center of the test tank, maintaining a distance of 960 mm from the outlet as well as the inlet, which is more than three times greater than the inlet diameter (i.e., 270.9 mm). This arrangement can prevent rapid flow caused by abrupt outlet and inlet cross-section changes. Additionally, the rock sample was prepared in the form of a sphere 40 mm in diameter and placed at the center of the test tank cross-section. This placement helps to minimize the impact of boundary effects and water turbulence resulting from the angles on the surface of the rock sample.

The average flow velocity at a point 100 mm upstream of the rock sample was measured using an LS-300A flow velocity meter (Weifang jinshui huayu information technology co., China, Shangdong Weifang). The section housing the rock samples experiences an increase in flow velocity due to the reduced overwater section. The scouring flow velocity of the rock samples is determined by multiplying the previously measured flow velocity by the coefficient of the flow velocity increase, denoted as K, due to the reduction in the overwater section, as defined in Equation (1):

$$K = \frac{A_1}{A_1 - A_\mathrm{r}} \tag{1}$$

where A_1 represents the cross-sectional area of water flow in the disintegration tank, and A_r denotes the cross-sectional area of the rock sample.

The water storage tank ensures a continuous water supply to the flow rate regulator throughout the testing process. Water constantly overflows from the top of the flow rate regulator during testing to maintain a stable flow rate within the disintegration tank. The adjustable height of the movable water tank allows for varying water flow rates within the disintegration tank. The disintegrated particle collection box serves the purpose of gathering particles disintegrated from the rock samples.

2.2. Rock Sample Preparation

The rock samples employed in this study were extracted from a highly weathered granite slope in Fuzhou city, as depicted in Figure 2. The pertinent physico-mechanical parameters are detailed in Table 1, with the XRD test results and mineral composition content presented in Figure 3 and Table 2, respectively.

Table 1. Basic physical indices of fragmentary highly weathered granite.

Natural Gravity/ kg·m^{-3}	Poisson's Ratio	Density/ g·cm^{-3}	Natural Moisture Content/%	Saturated Moisture Content/%
23.52	0.29	2.83	1.35	3.52

Table 2. Mineral composition of fragmented highly weathered granite.

Minerals	Kaolinite	Quartz	Albite	Galena	Others
Content/%	38.3	52.6	5.3	4.0	9.8

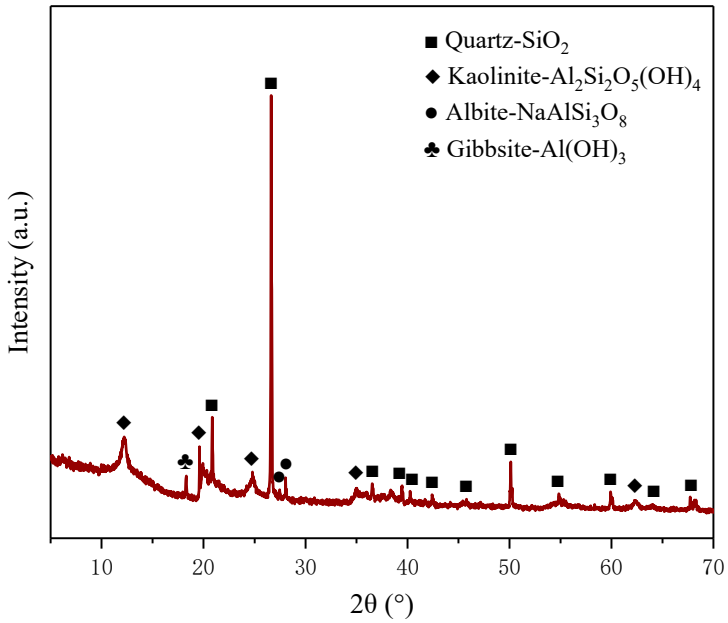

Figure 3. XRD test results for highly weathered granite.

Following the criteria outlined in the "Rock Testing Procedure for Water Conservancy and Hydropower Engineering" (DL/T5368–2007) [25], the rock samples were transformed into spherical samples with an approximate diameter of 40 mm, with each group comprising 10 samples, as visualized in Figure 4. To minimize sample dispersion, the NMR relaxation spectra for each group of samples exhibited similar porosities.

Figure 4. The highly weathered granite specimens.

2.3. Test Methods

To reveal the influence of immersion duration, flow rate, and the number of cycles on the disintegration of highly weathered granite subjected to scouring, the following experimental design was devised:

(1) Test 1: This test includes conducting disintegration tests on specimens exposed to varying scouring flow rates following different immersion durations. The aim is to determine the influence of the immersion length and scouring flow rate on the disintegration characteristics of the rock samples, as delineated in Table 3.

(2) Test 2: Building upon Test 1, multiple cycle tests are executed, varying the scouring flow rates applied to specimens initially immersed for 0, 2, 4, 12, and 24 h. The goal is to investigate the influence of the cycle count on the scouring and disintegration characteristics. The test program is presented in Table 4 (according to the preliminary experiment results, the heavily weathered granite has completed disintegration after 10 cycles, and no further disintegration has occurred).

Table 3. Experimental plan 1.

Immersion Duration/(h)	Flow Rate/(m/s)
0	0, 0.5, 1, 1.5, 2
2	0, 0.5, 1, 1.5, 2
4	0, 0.5, 1, 1.5, 2
10	0, 0.5, 1, 1.5, 2
24	0, 0.5, 1, 1.5, 2

Table 4. Experimental plan 2.

Immersion Duration/(h)	Flow Rate/(m/s)	Number of Cycles
0, 2, 4, 12, 24	0	1, 2, 3, 4, 5, 6, 7, 8, 9, 10
	0.5	1, 2, 3, 4, 5, 6, 7, 8, 9, 10
	1	1, 2, 3, 4, 5, 6, 7, 8, 9, 10
	1.5	1, 2, 3, 4, 5, 6, 7, 8, 9, 10
	2	1, 2, 3, 4, 5, 6, 7, 8, 9, 10

Adhering to the guidelines outlined in the "Rock Test Procedure for Water Conservancy and Hydropower Engineering" (SL/T264-2020) [26], the individual test steps unfold as follows:

(1) Test preparation: specimens were dried at 105 °C for 24 h, subsequently cooled to room temperature, and weighed.

(2) Test: Rock samples were placed in a disintegration tank and subjected to immersion treatment for the predetermined immersion duration. Following immersion, the test device was adjusted to ensure constant water flow within the disintegration tank, which was maintained for 2 h to facilitate flushing. The disintegrated particles were then collected, dried, sieved, and weighed. Finally, NMR spectroscopy was conducted on the flushed and disintegrated rock samples.

3. Cumulative Relative Disintegration under Scouring Action

In rock disintegration testing, particles with a size less than 2 mm are typically considered disintegrated particles [27]. After the scouring disintegration test, particles smaller than 2 mm were collected, and their mass was divided by the total sample mass to calculate the relative disintegration amount per cycle. The cumulative relative disintegration amount across multiple cycles is subsequently determined.

Figure 5 shows the changes in the cumulative relative disintegration of the rock samples under the different scouring flow rates, immersion durations, and cycle counts.

As shown in Figure 5, the cumulative relative disintegration of the rock samples increases with increasing immersion duration, cycle count, and scouring flow rate. However, once the scouring flow rate reaches a certain threshold, the cumulative relative disintegration ceases to exhibit significant changes (when the change from the last cycle is less than 1%).

Consequently, this paper defines the minimum flow rate at which the cumulative relative disintegration stabilizes, signifying that further increases in the flow rate yield negligible changes in disintegration. As depicted in Figure 5, the disintegration stabilization flow rate of the rock samples closely correlates with the immersion duration and cycle count.

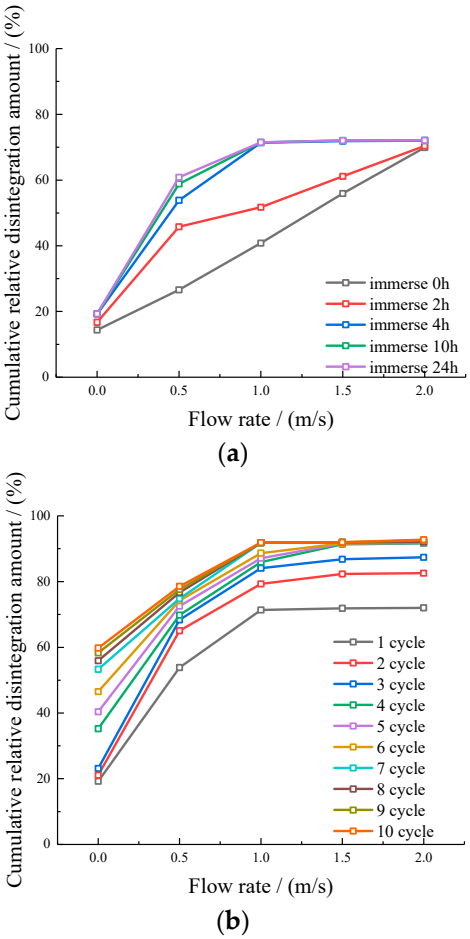

Figure 5. Cumulative relative disintegration at different flow rates. (**a**) Different durations of immersion; (**b**) different numbers of cycles.

4. Relationship between Disintegration Stabilization Flow Rate, Pore Space Variation, and Immersion Duration

4.1. Relationship between Disintegration Stabilization Flow Rate and Immersion Duration

Based on the results of the disintegration stabilization flow rate tests performed under varying cycle counts and immersion durations, the relationship between the disintegration stabilization flow rate and immersion duration is depicted in Figure 6.

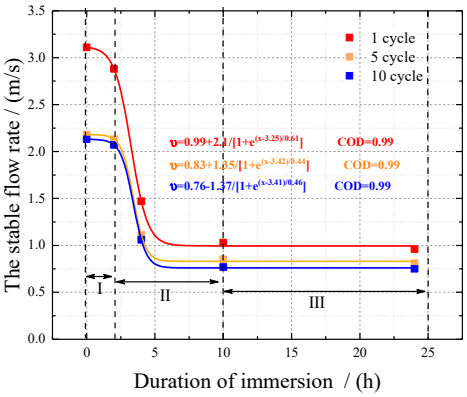

Figure 6. Relationship between the disintegration steady flow rate and immersion time.

As shown in Figure 6:

(1) As the initial immersion length of the rock samples increases, the disintegration stabilization flow rate generally exhibits three stages: an initial gradual decline (a maximum reduction of 0.62 m/s), a subsequent sharp reduction (a maximum reduction of 2.83 m/s), and eventual stabilization (a maximum reduction of 0 m/s).
(2) The disintegration stabilization flow rate, denoted as v_{cr}, is well fitted to the immersion duration, t. This relationship is defined by the following equation:

$$v_{cr} = a_1 + \frac{b_1}{1 + e^{(t-c_1)/d_1}} \quad (2)$$

where a_1, b_1, c_1, and d_1 represent fitting parameters dependent on the cycle count.

4.2. Relationship between Pore Changes and Immersion Time of Rock Samples

Previous research has indicated that as the immersion time increases, the internal porosity of the rock also increases, while the strength of the particle cementation decreases [28,29]. This could be a significant factor contributing to the alteration in the stabilization flow rate of disintegration among the rock samples with varying immersion times. To comprehensively analyze the patterns governing the change in the stabilization flow rate with immersion time and its underlying mechanisms, it is imperative to conduct an extensive investigation into the evolution of pore space within rock samples following scouring and disintegration under different immersion time conditions.

NMR spectroscopy is well suited for assessing pore changes within rocks [30,31]. The relaxation time and intensity of the NMR T2 relaxation spectrum correspond to the size and number of pores in the rock samples. The relaxation times [0.01 ms, 3 ms], [3 ms, 50 ms], and [50 ms, 10,000 ms] correspond to small, medium, and large pores within the rock samples, respectively [32]. The NMR tests were conducted on the rock samples after exposure to various immersion durations, and the relaxation spectra are provided in Figure 7. Given the similarity in trends under different flow rates, only the relaxation spectra for the scouring flow rates of 1 m/s and 2 m/s are presented, for brevity.

As depicted in Figure 7:

(1) With increasing immersion time, the peak intensity within the small pore range gradually increases, while the relaxation time steadily decreases. Conversely, the peak intensity and relaxation time for the medium and large pore ranges exhibit a gradual decrease.
(2) When the scouring flow rate surpasses the disintegration stabilization flow rate (from Figure 6, 1 m/s and 2 m/s for specimens with immersion lengths of 10 h and 4 h, respectively), the T2 relaxation spectra exhibit negligible changes with an extended immersion duration.

The aforementioned results indicate that under equivalent scouring flow rates, the number of larger and medium-sized pores in the rock samples decreases, while the number of small pores increases with extended immersion time. Subsequently, once the scouring flow rate surpasses the disintegration stabilization flow rate, the pores in the rock samples no longer undergo significant changes with prolonged soaking.

We established a correlation to further investigate the relationship between the immersion duration and alteration in rock sample porosity following scouring disintegration. This correlation was based on the results of scouring disintegration tests conducted on the rock samples and porosity measurements obtained via NMR technology after the scouring process. The resulting relationship between the change in the cumulative relative disintegration and rock sample porosity over different immersion durations is depicted in Figure 8.

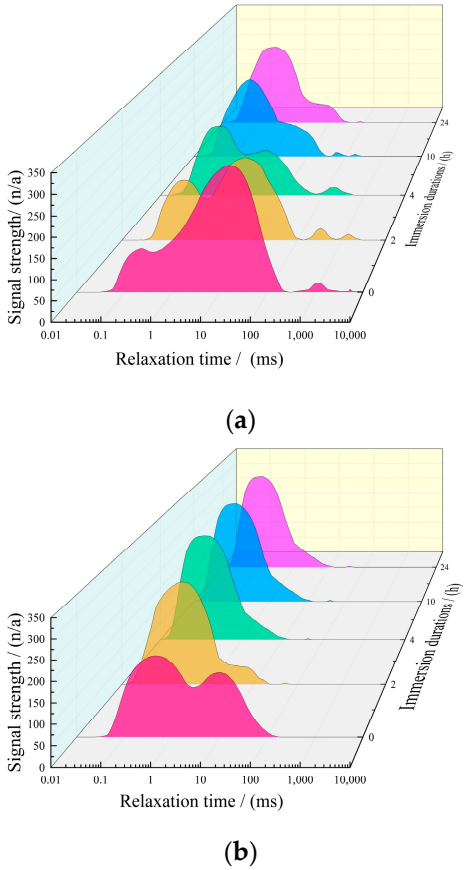

Figure 7. T_2 relaxation spectra under different scouring flow rates and immersion durations. (**a**) Flow rate 1 m/s; (**b**) flow rate 2 m/s (Different colors correspond to different immersion durations, as shown in the axes).

As shown in Figure 8:

(1) The disintegration of the rock samples under the action of scouring can be categorized into three stages as the immersion time increases: initial rapid disintegration (stage I), medium-term gradual disintegration (stage II), and late stabilization (stage III). The characteristics of these stages become more pronounced with lower scouring flow rates and shorter rapid disintegration stages with higher scouring flow rates.

(2) During the initial rapid disintegration stage, an extended immersion time led to a substantial increase in the cumulative disintegration of the rock samples, accompanied by a marked decrease in porosity (as shown in Figure 8a, the cumulative relative disintegration volume increased by 32.4%, and the porosity decreased by 0.03). Conversely, during medium-term gradual disintegration, both the cumulative disintegration amount and rock sample porosity gradually increased as the immersion time increased. Once the disintegration stabilization stage was reached, neither the cumulative disintegration amount nor the rock sample porosity demonstrated significant changes.

To gain further insight into the evolution characteristics of the rock samples with different pore sizes during scouring and disintegration, we utilized the following formula, based on experimental findings, to compute the proportions of large (D_{mac}), medium (D_{mec}), and small (D_{mic}) pores in the rock samples after scouring and disintegration with varying immersion times:

$$\begin{aligned} D_{mac} &= \frac{V_{mac}}{V_{total}} \times 100\% \\ D_{mes} &= \frac{V_{mes}}{V_{total}} \times 100\% \\ D_{mic} &= \frac{V_{mic}}{V_{total}} \times 100\% \end{aligned} \quad (3)$$

where V_{total}, V_{mac}, V_{mec}, and V_{mic} represent the total pore volume, large pore volume, medium pore volume, and small pore volume, respectively, of the rock samples after flushing. The relationship between the percentage of the different pore volumes in the rock samples and the immersion duration is presented in Figure 9.

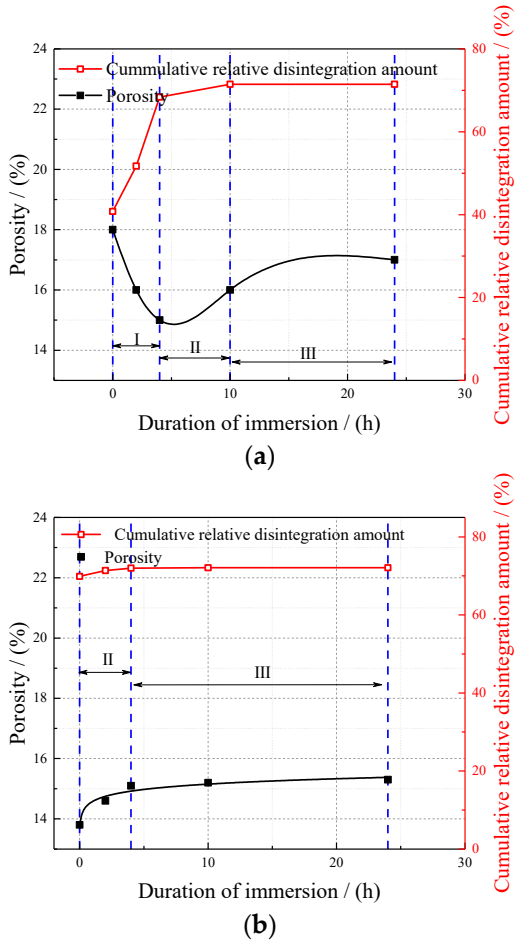

Figure 8. Relationships between porosity, cumulative relative disintegration, and immersion time. (**a**) Flow rate 1 m/s; (**b**) flow rate 2 m/s.

As shown in Figure 9:

(1) During the initial rapid disintegration stage, as the immersion time increases, the percentage of the large pore volume in the rock samples sharply decreases (as shown in Figure 9a, a maximum reduction of 81.23%), while the percentage of the medium pore volume increases significantly (a maximum increase of 54.05%), with only minimal change in the percentage of the small pore volume.

(2) In the medium-term gradual disintegration stage, the proportion of large pores in the samples is minimal. With prolonged immersion time, the proportion of medium pores in the samples sharply decreases (as shown in Figure 9b, a maximum reduction of 52.48%), while the proportion of small pores in the samples increases significantly.

(3) In the late stabilization stage, the volume fraction of the large pores in the rock samples remains very low, and the volume fraction of the medium and small pores shows little change with increasing immersion time.

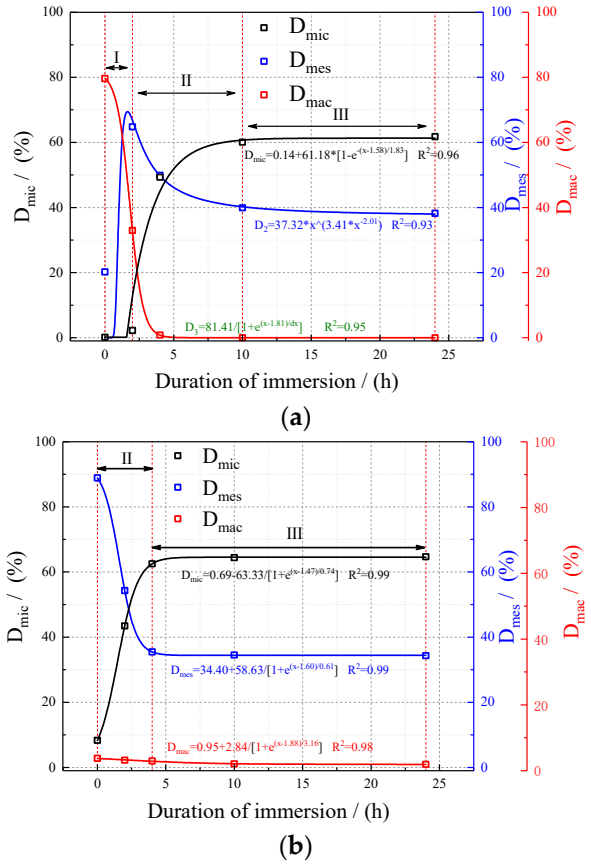

Figure 9. Rate of change in the pore volume per unit of time. (**a**) Flow rate 1 m/s; (**b**) flow rate 2 m/s.

The above results show that sharp disintegration primarily stems from the detachment of particles surrounding the large pores within the rock samples. After sharp disintegration occurs, there is a noticeable reduction in the size of the large pores within the rock samples, which significantly weakens the disintegration process. During this stage, the medium-sized pores that initially increase in size during sharp disintegration tend to transition into large pores. This transition is characterized by the continued detachment of particles around these pores, resulting in a decrease in the medium-sized pores and a slower disintegration process. Simultaneously, water-rock interactions induce a sharp increase in the number of small pores. As disintegration progresses into the stabilization stage, the rock samples experience a gradual increase in the volume of small and medium-sized pores under the continued influence of water-rock interactions.

5. Relationship between Disintegration Stabilization Flow Rate, Pore Space Variation, and Number of Cycles

5.1. Relationship between Disintegration Stabilization Flow Rate and Number of Cycles

Based on the results of the disintegration stabilization flow rate tests under different immersion durations, scouring flow rates, and cycle times for the test samples, the relationship between the disintegration stabilization flow rate and cycle times is depicted in Figure 10. This is not discussed because the number of cycles has little effect on the stable flow rate of disintegration after the immersion time of the test rock sample surpasses 10 h.

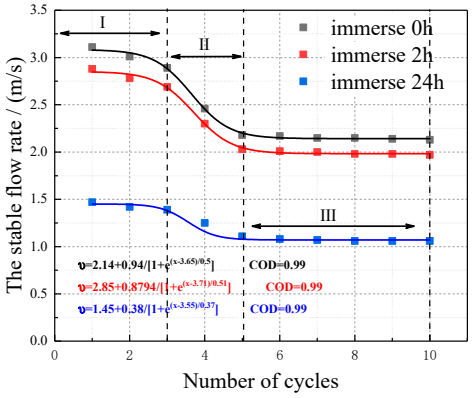

Figure 10. Relationships between different pore volume percentages and immersion times.

As shown in Figure 10:

(1) The disintegration-stabilized flow rate of the rock samples subjected to different immersion durations generally exhibits three stages: an initial slow decrease, a sharp decrease in the middle stage, and stabilization in the later stage as the number of cycles increases.

(2) As the immersion time decreased, the impact on the disintegration stabilization flow rate became more pronounced with increasing cycles during the rapid reduction stage. Notably, the disintegration-stabilized flow rate of the rock samples in this study remained relatively constant when the immersion duration reached 10 h.

(3) The disintegration stabilization flow rate (v_{cr}) and the number of cycles (N) strongly correlated with the immersion duration, as described by the following relationship:

$$v_{cr} = a_2 + \frac{b_2}{1 + e^{(N - c_2)/d_2}} \quad (4)$$

where a_2, b_2, c_2, and d_2 are the fitting parameters related to the immersion duration.

5.2. Relationship between Pore Changes and Cycle Times of Rock Samples

NMR spectroscopy was conducted on the relaxation spectra of the rock samples following disintegration by flushing for various numbers of cycles, as illustrated in Figure 11. Due to the similar trends in the relaxation spectra at different flow rates, only the relaxation spectra of the rock samples subjected to 4 h of immersion and a scouring flow rate of 1 m/s with varying numbers of cycles of scouring and disintegration are presented for brevity.

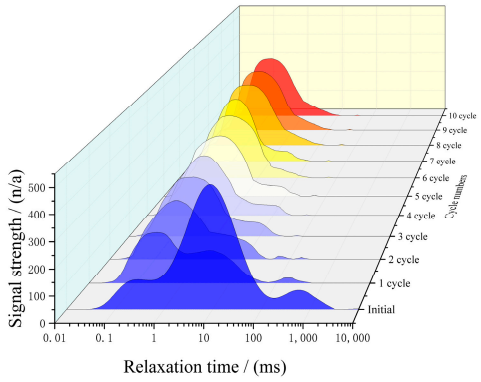

Figure 11. T_2 relaxation spectra under different scouring flow rates and immersion durations (Different colors correspond to different immersion durations, as shown in the axes).

As shown in Figure 11:

(1) As the number of cycles increases, the peak intensity of the small pore interval gradually increases, and the relaxation time progressively decreases. Conversely, the peak intensity and relaxation time of the medium and large pore intervals decrease.
(2) After more than six cycles (approaching a disintegration-stabilized flow rate of 1 m/s), the T2 relaxation spectra cease to exhibit significant changes with an increasing number of cycles.

The results above indicate that when the initial immersion length and scouring flow rate are held constant, an increase in the number of cycles leads to a decrease in the large and medium pores in the rock samples, while the number of small pores increases. However, once the number of cycles surpasses a certain threshold, the pores in the rock samples (large, medium, or small) no longer undergo significant changes during scouring and disintegration.

To further investigate the relationship between the number of cycles and the changes in the porosity of the rock samples following scour disintegration, we established a relationship between the cumulative relative disintegration amount and the porosity of the rock samples with the number of cycles, as shown in Figure 12.

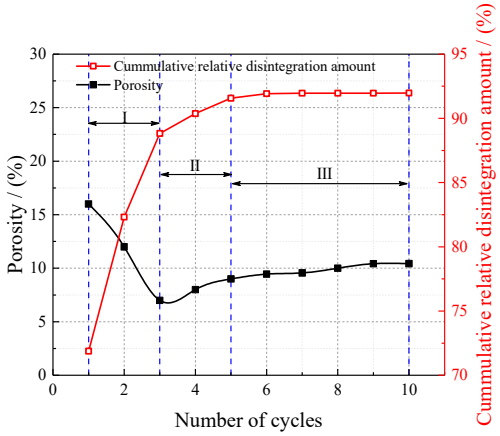

Figure 12. T_2 relaxation spectra at different numbers of wetting–drying cycles.

As shown in Figure 12:

(1) As the number of cycles increases, the scouring disintegration of the rock samples can be categorized into three stages: initial sharp disintegration (stage I), medium-term slow disintegration (stage II), and late stabilization (stage III).
(2) During the rapid disintegration stage, the cumulative disintegration amount and the porosity of the rock samples sharply decrease with an increasing number of cycles. In the slow disintegration stage, these parameters increase gradually with increasing cycle number, and in the disintegration stabilization stage, there is only a minor increase in both the cumulative disintegration and porosity.

To further reveal the variation in the different scales of pore volume with the number of cycles during the process of scouring and the disintegration of rock samples, we derived the relationship between the percentage of different pore volumes in the rock samples after scouring and disintegration and the number of cycles. This relationship is outlined in Section 4.2 and illustrated in Figure 13.

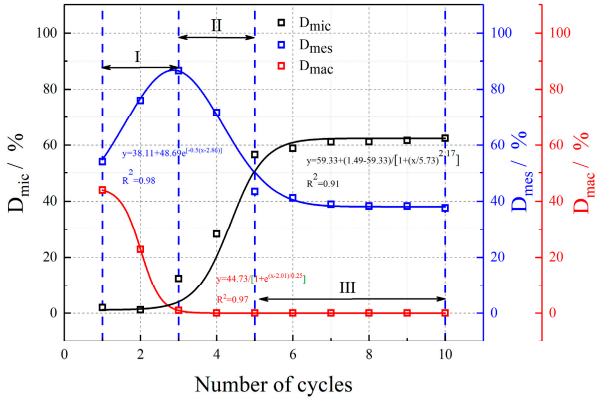

Figure 13. Relationships between the porosity, cumulative relative disintegration, and number of wetting–drying cycles.

As shown in Figure 13:

(1) During the rapid disintegration stage, an increase in the number of cycles leads to a sharp decrease in the percentage of the large pore volume in the sample, a significant increase in the percentage of the medium pore volume, and only minor changes in the percentage of the small pore volume.

(2) In the medium-term slow disintegration stage, the proportion of large pores in the rock samples is minimal. With an increasing number of cycles, the pore volume in the rock samples decreases sharply, while the percentage of small pores increases significantly.

(3) In the late stabilization stage, the rock samples predominantly contain small pores, and the volume shares of the medium and small pores remain relatively stable with an increasing number of cycles.

These results further highlight that sharp disintegration primarily arises from the detachment of particles surrounding the large pores in the rock samples. Following sharp disintegration, the large pores in the rock samples decrease in number, leading to a noticeable weakening of the disintegration process. During the joint action of water-rock interactions and scouring, some of the medium pores that increased during the sharp disintegration stage evolved into large pores, while the surrounding particles still underwent exfoliation. This transformation results in a reduction in the number of medium pores and a decrease in disintegration. Additionally, the water-rock interactions lead to dramatic increases in the small pores. As disintegration progresses into the stabilization stage, the rock samples subjected to prolonged immersion experience a gradual increase in both the medium and small pore volumes due to ongoing water-rock interactions.

6. Formation Mechanism of Rock Sample Disintegration under Scouring Action

The pores within the rock samples serve as pathways for the solution to penetrate the interior of the rock samples, where they undergo physicochemical reactions that alter mechanical parameters such as the particle bond strength. As demonstrated in Table 2, the highly weathered granite employed in this paper's test contains internal muddy cement and clay minerals, predominantly kaolinite, which are readily soluble in water. Upon immersion in water, the mud cement dissolved, increasing the pore volume and initial pore expansion. With prolonged immersion, the water-rock interactions intensify, causing a further increase in the internal rock porosity and pore expansion. The strength of the cement between the particles surrounding the larger pores decreased, allowing them to be eroded by the lower scouring flow rate generated by shear forces from the parent body. This, in turn, led to the additional expansion of the original pore space, ultimately providing more pathways for water to infiltrate the rock.

The disintegration of rock under scouring is closely linked to the shear strength (τ_f) between the constituent rock particles and the shear force (τ) generated by water scouring. The particle-induced shear force (τ_c) of water scouring can be calculated using Equation (5):

$$\tau_c = \frac{2}{[5.75\lg(30.2\frac{y_d}{K_s}\chi)]^2} C_2 \tau_f \quad (5)$$

where K_s represents the particle surface roughness, χ is a function associated with the particle surface roughness, and C_2 is a parameter linked to the resistance against the water flow direction. In this paper, the rock samples undergo scouring tests under consistent environmental conditions, and the abovementioned parameters remain constant throughout. Additionally, yd represents the particle diameter, and since this paper exclusively includes particles with sizes less than 2 mm for the disintegration analysis (which is also the current standard for rock disintegration tests), we can treat this as an unchanging constant in subsequent analyses.

The shear strength (τ_f) between the rock particles can be calculated using a reference to the M-C criterion [33]:

$$\tau_f = \sigma_p f + c_p \quad (6)$$

where σ_p and c_p denote the normal stress and cementation force between the particles, respectively, and f represents the friction coefficient between the particles. For the surface layer of the rock and soil body on the slope, which is not subject to additional loads, the normal stress (σ_p) between the particles is negligible and can be disregarded in the calculations. Consequently, the particle shear resistance against scouring and disintegration primarily stems from the bond strength (c_p) between the particles. Assuming the same type of cement, c_p remains consistent, with the bond force between the particles is determined by their bonding area.

The scouring shear stress of water flow on the surface particles of the rock samples increases with increasing flow rate. According to Equation (5), the impacts of the immersion length and the number of cycles on the disintegration stabilization flow rate of the rock samples can be summarized as follows:

(1) During the rapid disintegration stage, the particles surrounding the large pores in the rock samples exhibit the lowest shear resistance to scour disintegration, as the large pores diminish the cemented area between them and the surrounding particles. Consequently, disintegration primarily affects the particles surrounding the large pores. The volume ratio of the large pores in the rock samples sharply decreases during the rapid disintegration stage, as observed in Figures 9 and 13.

(2) As disintegration progresses, the amount of macroporous space significantly decreases, resulting in a substantial increase in the cemented area between the remaining surface particles and their surrounding counterparts compared to that of the particles around the macroporous spaces. The bonding force between the particles increases accordingly, and disintegration halts when the bonding force equals the shear force of the water flow scouring. The flow rate corresponding to this cessation point is the disintegration stabilization flow rate. Therefore, the phenomenon of a disintegration stabilization flow rate, as shown in Figure 5, is observed in the rock samples subjected to various immersion lengths and cycle times.

(3) As the initial immersion length of the rock samples increases, the water-rock interactions intensify, increasing the pore volume. Larger pores facilitate solution infiltration, enhancing the water-rock interactions. Consequently, the rock sample pore space enlarges with longer initial immersion times, reducing the cemented area between the particles surrounding the large pore spaces. This reduction weakens the resistance to water scouring, decreasing the disintegration stabilization flow rate, as illustrated in Figure 6.

(4) Similarly, wet-dry cycles enlarge the rock sample pores, causing the disintegration stabilization flow rate to decrease with an increasing number of cycles, as shown in Figure 10.
(5) Although both immersion and the wet-dry cycles gradually increase the number of the rock sample pores, shorter immersion durations or fewer wet-dry cycles do not significantly expand the large pores. The large pores in the rock samples undergo significant expansion only after reaching a certain accumulation of damage during immersion or the wet-dry cycles. Thus, the disintegration stabilization flow rate exhibits the characteristics of an initial slow decrease, a sharp decrease in the middle stage, and ultimately stabilization, as demonstrated in Figures 6 and 10.
(6) After a certain duration of immersion or a specific number of wet-dry cycles, the medium and large pores in the rock samples evolve into large pores. In this paper, the immersion duration and cycle number reached the limits at which the small pores could not transform into large pores. Consequently, the disintegration stabilization flow rate ceases to decrease significantly after surpassing a specific immersion duration or cycle number, as depicted in Figures 6 and 10.

7. Conclusions

In this study, we utilized a custom-designed disintegration test device to conduct experiments on highly weathered granite specimens with varying immersion durations and flow rates and subjected them to different numbers of cycles. The pore changes in the disintegrated rock samples were analyzed using nuclear magnetic resonance (NMR) technology, leading to the following key conclusions:

(1) The cumulative relative disintegration of highly weathered granite increases as the scouring flow rate, immersion time, and cycle number increase. Once a specific threshold in the scouring flow rate is reached, the cumulative relative disintegration stabilizes, giving rise to a flow rate associated with disintegration stabilization. This flow rate demonstrated a robust correlation with either the immersion duration or cycle number.
(2) Highly weathered granite disintegration exhibits a tripartite progression comprising an initial phase of rapid disintegration, a subsequent intermediate phase of gradual disintegration, and a final phase of stabilization, all of which are associated with lengthened immersion times (or cycle numbers). Correspondingly, alterations in the flow rate associated with disintegration stabilization exhibit a comparable triphasic pattern as the immersion duration (or cycle number) increases.
(3) In the rapid disintegration stage, an extended immersion time (or higher cycle number) precipitates a pronounced reduction in the volume ratio of the large pores within the rock samples while simultaneously resulting in a substantial increase in the volume ratio of the medium pores, with negligible changes observed in the volume ratio of the small pores. During the slow disintegration stage, an increase in the immersion time (or cycle number) leads to a marked reduction in the volume ratio of the medium pores, concomitant with a notable increase in the volume ratio of the small pores. Within the disintegration and stabilization stage, large pores become scarce. In contrast, the volume ratio of the medium to small pores exhibits relative stability, even as the immersion time (or cycle number) increases.
(4) When exposed to scouring, the disintegration of highly weathered granite predominantly occurs in proximity to the large pores. The changes in the disintegration characteristics induced by the variations in the immersion times (or cycle numbers) are primarily attributed to the dynamic shift in the relative volume of the large pores within the rock samples.

Author Contributions: Conceptualization, X.H., C.L. and C.W.; methodology, X.H. and C.L.; formal analysis, X.H.; resources, C.L.; data curation, X.H.; writing—original draft preparation, X.H.; writing—review and editing, C.L., X.Z. and Z.W.; project administration, C.L. and X.Z.; funding acquisition, C.L. and X.Z. All authors have read and agreed to the published version of the manuscript.

Funding: This research was funded by National Natural Science Foundation of China (41272300; 42202301); the Major Projects of Scientific and Technological Innovation of CRTG (2018-53), and Natural Science Foundation of Fujian Province (2020J05133).

Data Availability Statement: The original contributions proposed in this study are included in the article. Any further inquiries can be directed to the corresponding author.

Conflicts of Interest: The authors declare no conflicts of interest.

References

1. Lee, Y.F.; Chi, Y.Y. Rainfall-induced landslide risk at Lushan, Taiwan. *Eng. Geol.* **2011**, *123*, 113–121. [CrossRef]
2. Gautam, T.P.; Shakoor, A. Comparing the slaking of clay-bearing rocks under laboratory conditions to slaking under natural climatic conditions. *Rock Mech. Rock Eng.* **2016**, *49*, 19–31. [CrossRef]
3. Wang, W.; Xu, Q.; Zheng, G.; Li, J.; Luo, B. Centrifugal model tests on sliding failure of gentle debris slope under rainfall. *Rock Soil Mech.* **2016**, *37*, 87–95. [CrossRef]
4. Sarman, R.; Shakoor, A.; Palmer, D.F. A multiple regression approach to predict swelling in mudrocks. *Bull. Assoc. Eng. Geol.* **1994**, *31*, 107–121. [CrossRef]
5. Kıncal, C.; Koca, M.Y.; Ozden, G.; Demirbasa, N. Fractal parameter approach on weathering grade determination of Çeşme (Izmir, Turkey) tuffs. *Bull. Eng. Geol. Environ.* **2011**, *70*, 331. [CrossRef]
6. Ghobadi, M.H.; Mousavi, S. The effect of pH and salty solutions on durability of sandstones of the Aghajari Formation in Khouzestan province, southwest of Iran. *Arab. J. Geosci.* **2014**, *7*, 641–653. [CrossRef]
7. Zhang, Z.; Gao, W.; Huang, J.; Ouyang, S.; Zhang, Z. Swelling characteristics of red sandstone under cyclic wetting and drying. *Geotech. Geol. Eng.* **2020**, *38*, 4289–4306. [CrossRef]
8. Yavuz, H. Effect of freeze–thaw and thermal shock weathering on the physical and mechanical properties of an andesite stone. *Bull. Eng. Geol. Environ.* **2011**, *70*, 187–192. [CrossRef]
9. Wu, D.; Liu, H.; Wang, G. Laboratory experimental study of slaking characteristics of red-bed soft rock. *Chin. J. Rock Mech. Eng.* **2010**, *29*, 4173–4179.
10. Dhakal, G.; Yoneda, T.; Kato, M.; Kaneko, K. Slake durability and mineralogical properties of some pyroclastic and sedimentary rocks. *Eng. Geol.* **2002**, *65*, 31–45. [CrossRef]
11. Chai, Z.; Zhang, Y.; Zhang, X. Experimental investigation on correlation with slake durability and mineral composition of mudstone. *J. China Coal Soc.* **2015**, *40*, 1188–1193. [CrossRef]
12. Erguler, Z.A.; Shakoor, A. Relative contribution of various climatic processes in disintegration of clay-bearing rocks. *Eng. Geol.* **2009**, *108*, 36–42. [CrossRef]
13. Zhang, Z.; Gao, W.; Chen, Q.; Zhang, Z. A lateral unconfined swelling test for swelling rocks. *Adv. Mater. Sci. Eng.* **2018**, *2018*, 1823541. [CrossRef]
14. Vergara, M.R.; Triantafyllidis, T. Swelling behavior of volcanic rocks under cyclic wetting and drying. *Int. J. Rock Mech. Min. Sci.* **2015**, *80*, 231–240. [CrossRef]
15. Zhang, D.; Chen, A.; Su, Y.; Duan, H.; Wang, R.; Liu, G. Influence of hydrothermal environment on the disintegration characteristics of different purple parent rocks. *Acta Pedol. Sin.* **2013**, *50*, 643–651. [CrossRef]
16. Zhao, J.; Lu, C.; Deng, L.; Liu, G. Impacts of simulated acid solution on the disintegration and cation release of purple rock (mudstone) in Southwest China. *Geomorphology* **2018**, *316*, 35–43. [CrossRef]
17. Zhang, D.; Chen, A.; Liu, G. Laboratory investigation of disintegration characteristics of purple mudstone under different hydrothermal conditions. *J. Mt. Sci.* **2012**, *9*, 127–136. [CrossRef]
18. Zhang, Z.T.; Gao, W.H. Effect of different test methods on the disintegration behaviour of soft rock and the evolution model of disintegration breakage under cyclic wetting and drying. *Eng. Geol.* **2020**, *279*, 105888. [CrossRef]
19. Zhang, Z.T.; Gao, W.H.; Zeng, C.F.; Tang, X.Y.; Wu, J. Evolution of the disintegration breakage of red-bed soft rock using a logistic regression model. *Transp. Geotech.* **2020**, *24*, 100382. [CrossRef]
20. Zhao, G.; Visser, P.J.; Peeters, P.; Vrijling, J.K. Headcut migration prediction of the cohesive embankment breach. *Eng. Geol.* **2013**, *164*, 18–25. [CrossRef]
21. Wang, L.; Chen, G.; Zhan, Q.; Wang, S. Critical incipient motion of slope soil under thin layer flow scouring. *J. Civil Environ. Eng.* **2022**, 1–11. Available online: https://kns.cnki.net/kcms/detail/50.1218.TU.20220124.1631.008.html (accessed on 26 January 2022).
22. Wu, Q.; Wang, C.; Song, P.; Zhu, H.; Ma, D. Rainfall erosion experiment for steep loess slope and fluid-soil coupling simulation with PFC3D. *Rock Soil Mech.* **2014**, *35*, 977–985. [CrossRef]

23. Yan, L.; Liu, P.; Peng, H.; Kašanin-Grubin, M.; Lin, K. Laboratory study of the effect of temperature difference on the disintegration of redbed softrock. *Phys. Geogr.* **2019**, *40*, 149–163. [CrossRef]
24. Zhao, Y.R.; Yang, H.Q.; Huang, L.P.; Chen, R.; Chen, X.S.; Liu, S.Y. Mechanical behavior of intact completely decomposed granite soils along multi-stage loading–unloading path. *Eng. Geol.* **2019**, *260*, 105242. [CrossRef]
25. *DL/T5368-2007*; Rock Testing Procedure for Water Conservancy and Hydropower Engineering. National Development and Reform Commission, People's Republic of China: Beijing, China, 2007.
26. *SL/T264-2020*; Code for Rock Tests in Water and Hydropower Projects. Ministry of Water Resources of People's Republic of China: Beijing, China, 2020.
27. Li, K.; Zhao, X.; Xiao, D.; Li, J. Mechanism of silty mudstone slaking aggravated by acid rain-induced chemical damage. *Rock Soil Mech.* **2020**, *41*, 2693–2702. [CrossRef]
28. Armand, G.; Conil, N.; Talandier, J.; Seyedi, D.M. Fundamental aspects of the hydromechanical behaviour of Callovo-Oxfordian claystone: From experimental studies to model calibration and validation. *Comput. Geotech.* **2017**, *85*, 277–286. [CrossRef]
29. Sørensen, E.S.; Clausen, J.; Damkilde, L. Finite element implementation of the Hoek–Brown material model with general strain softening behavior. *Int. J. Rock Mech. Min. Sci.* **2015**, *78*, 163–174. [CrossRef]
30. Yu, J.; Zhang, X.; Cai, Y.; Liu, S.; Tu, B.; Fu, G. Meso-damage and mechanics properties degradation of sandstone under combined effect of water chemical corrosion and freeze-thaw cycles. *Rock Soil Mech.* **2019**, *40*, 455–464. [CrossRef]
31. Kong, L.; Sayem, H.M.; Tian, H. Influence of drying–wetting cycles on soil-water characteristic curve of undisturbed granite residual soils and microstructure mechanism by nuclear magnetic resonance (NMR) spin-spin relaxation time (T_2) relaxometry. *Canadian Geotech. J.* **2018**, *55*, 208–216. [CrossRef]
32. Qin, Q.; Li, K.; Li, M.; Li, W.; Liu, B. Study on the deterioration mechanism of dolomite microscopic damage based on NMR technique. *Chin. J. Rock Mech. Eng.* **2022**, *41*, 2944–2954. [CrossRef]
33. Zhao, J.S.; Duan, S.Q.; Chen, B.R.; Li, L.; He, B.G.; Li, P.X.; Liu, G.F. Failure mechanism of rock masses with complex geological conditions in a large underground cavern: A case study. *Soil Dyn. Earthq. Eng. J.* **2024**, *177*, 108439. [CrossRef]